Received: 5 May 2020 | Revised: 23 June 2020 | Accepted: 24 June 2020

DOI: 10.1002/er.5777

RESEARCH ARTICLE

INTERNATIONAL JOURNAL OF ENERGY RESEARCH WILEY

Methanol and proton transport through chitosan-phosphotungstic acid membranes for direct methanol fuel cell

Andrea Zaffora | Francesco Di Franco | Emanuele Gradino | Monica Santamaria

Dipartimento di Ingegneria, Università degli Studi di Palermo, Palermo, Italy

Correspondence
Francesco Di Franco, Dipartimento di Ingegneria, Università degli Studi di Palermo, Viale delle Scienze, Ed. 6, Palermo 90128, Italy.
Email: francesco.difranco@unipa.it

Funding information
Ministry of Education, University and Research

Summary

Composite chitosan-phosphotungstic acid membranes were synthesized by ionotropic gelation. Their liquid uptake is higher for thin membranes (23 ± 2 μm), while it is lower (~70%) for thicker membranes (50-70 μm). Polarization curves recorded using single module fuel cell at 70°C allowed to estimate a peak power density of 60 mW cm^{-2} by using 1 M as methanol and low Pt and Pt/Ru loadings (0.5 and 3 mg cm^{-2}) at the cathode and at the anode, respectively. Electrochemical impedance spectroscopy was used to estimate the membrane conductivity and to model the electrochemical behavior of methanol electrooxidation inside the fuel cell revealing a two-step mechanism mainly responsible of overall kinetic losses. Transport of methanol inside the membrane was studied by potentiostatic measurements, allowing to estimate a methanol diffusivity of 3.6×10^{-6} cm^2 s^{-1}.

KEYWORDS

chitosan, direct methanol fuel cells, methanol permeability, phosphotungstic acid, proton conductivity

1 | INTRODUCTION

Direct methanol fuel cells (DMFCs) have attracted much attention due to several advantages, like a quick start-up at low temperature, a high energy density, rich sources, easy transportation, and storage of fuel.[1-4] However, two major obstacles that currently prevent the widespread commercial applications of DMFCs are (a) the low activity of reported methanol electrooxidation catalysts to date and (b) crossover of methanol through the polymer electrolyte membrane that leads to a decrease in voltage efficiency.[5-9] In order to overcome these problems, much attention has been paid to study the methanol electrooxidation mechanism on different catalysts,[10,11] and to develop polymer electrolyte membrane matching a high conductivity with a low methanol permeability.[12-17]

Nafion membranes are commonly used as polymer electrolytes due to their high proton conductivity and to their chemical, mechanical, and thermal stability,[18] although they suffer of relatively high methanol crossover, high manufacturing costs, and they are not environmentally friendly. As alternative to perfluorinated membranes as Nafion, chitosan (CS) represents one of the most rationale choice in the vast world of proton exchange membrane (PEM) for DMFCs because of a promising low methanol permeability,[19-21] joined to unique features of hydrophilicity, biocompatibility, biodegradability, and cost-effectiveness.[22] Moreover, CS backbone contains free amine groups that can be protonated, making CS a polycation that can electrostatically interact with polyanions to prepare tailored membranes for fuel cells.[22,23] However, CS suffers from a quite low

proton conductivity that can heavily limit its use in DMFCs. Therefore, a commonly exploited strategy to enhance its proton conductivity is the introduction inside CS chains of acids and salts of heteropolyanions.

Heteropolyacids (HPAs) are well-known superionic proton conductors in the fully hydrated states, and are widely used as proton conductor solid electrolytes as well as to enhance proton conductivity of CS membranes.[24-27] Cui et al proposed polyelectrolyte complexes of CS and an HPA (phosphotungstic acid [PTA]) to be used as PEM in DMFCs demonstrating good swelling properties, good proton conductivity, and low methanol permeability,[28] as also done by Wu et al whose membranes allowed to get a peak power density of 16 mW cm^{-2}.[29] On the other hand, HPAs can facilitate the oxidative removal of CO_{ads} poisoning species for methanol oxidation and desorption of O_{ads} species for oxygen reduction reaction on Pt catalysts,[30,31] thus their presence at the electrode/polymer electrolyte interface can reduce the kinetic losses due to the cell reaction.

The efficacy of this approach is limited by leaching phenomena that can occur during DMFCs operations with consequent detrimental effect on the proton conductivity and on overall device performances. In this regard, we proposed an efficient procedure (ie, ionotropic gelation process) to obtain CS-HPA composite membranes that were, up to now, successfully tested as proton conductors just in low temperature H_2 fed fuel cells.[32-35] CS is dissolved in an aqueous acetic acid solution, where it is protonated and behaves like a cationic polyelectrolyte and can be ionically cross-linked by anionic species. Therefore, using a porous medium previously embedded with HPA for the slow release of Keggin anions induces the crosslinking with protonated chitosan to occur on its surface allowing to prepare flat, homogenous and free-standing membranes, whose thickness can be finely tuned by tuning the contact (ie, reticulation) time.[33] According to the scanning electron microscopy (SEM) images, the membranes are very compact without microvoids, thus being very promising as efficient barrier toward methanol crossover.

In this work, we prepared by ionotropic gelation process CS/PTA composite membranes of different thickness to be tested, for the first time, as polymer electrolytes for DMFC. The membranes were characterized by liquid uptake (using a water-methanol solution); SEM was used to get information on the membrane's morphology and thickness; then, they were tested in a single module methanol/O_2 fuel cell to explore the possibility to use them as efficient proton conductors in DMFCs. Electrochemical impedance spectroscopy (EIS) was used to get information about the proton conductivity of the membrane as well as to obtain a comprehensive understanding of the kinetics of the methanol oxidation reaction (MOR) in the DMFC. Membrane methanol permeability was estimated by in-cell measurements under the operating conditions of a DMFC.

2 | EXPERIMENTAL SECTION

2.1 | Membrane synthesis

Chitosan powder, acetic acid, and $H_3PW_{12}O_{40} \cdot xH_2O$ were supplied by Sigma Aldrich.

Membranes were synthesized by ionotropic gelation process on a porous support previously impregnated by an HPA as described elsewhere.[34] A 2 wt/vol% chitosan in acetic acid aqueous solution and a porous medium previously impregnated with PTA were put in contact for different times to induce CS reticulation through cross-linking reaction. This reticulation step was used to control membrane thickness: a longer reticulation time led to a thicker membrane. The porous medium employed in this work is an etched aluminum foil, anodized under potentiostatic condition at 75 V for 3 hours in 0.1 M ammonium biborate tetrahydrate solution (ABE, $[NH_4]_2B_4O_7{\cdot}4H_2O$) (pH ~9). The latter is easier to handle than brittle anodic alumina membranes employed in previous works.[33] The structural and morphological characterizations of the membranes revealed that employing a different porous medium does not affect the quality and composition of the membranes (see Section 3.1 and Supplementary Material).

Membrane functionalization step was then performed by immersing the obtained membrane in PTA-water solution (0.38 M) for 24 hours in order to increase the HPA content in the ion-exchange membrane, thus increasing the membrane proton conductivity.

2.2 | SEM characterization

SEM analysis was performed by using a Philips XL30 ESEM coupled with EDX equipment. Prior to imaging, several pieces of each sample were fixed on the metal stubs with Ag conductive paste. SEM images and membrane thicknesses are reported in the Supplementary Material.

2.3 | Liquid uptake

Membrane's liquid uptake was estimated through the following relationship:

$$\mathrm{WU}\,(\%) = \frac{W_{\mathrm{wet}} - W_{\mathrm{dry}}}{W_{\mathrm{dry}}} \times 100. \quad (1)$$

where W_{dry} is the membrane weight after the drying procedure: once synthetized (without functionalization step), the membrane is washed with distilled water to remove any chitosan/acetic acid aqueous solution traces and then dried in atmosphere for 24 hours. After a 24-hour immersion in distilled water or 1 M methanol aqueous solution, the solution excess is removed from the membrane which is weighted to estimate W_{wet}. Every liquid uptake measurement was repeated three times for all the characterized membranes.

2.4 | Fuel cell performances

The electrodes were prepared by spraying a catalytic ink onto a commercial gas diffusion layer Sigracet—24 BC (by SGL group).[36] Two different catalysts were used: for the anodic reaction (methanol oxidation) the employed catalytic ink was obtained by mixing 60 wt% Pt-Ru/C catalyst was mixed with 33 wt% Nafion ionomer (IonPower, 5 wt% solution) under sonication and deposited by a doctor blade technique onto the backing layer with a final Pt/Ru loading of 3 mg·cm^{-2}. For the cathodic reaction (oxygen reduction), the employed catalytic ink was obtained by mixing the 40 wt% Pt/C (Johnson Matthey) with a 33 wt% of dry Nafion (5 wt% hydro-alcoholic solution, IonPower—LQ1105) with a Pt loading of 0.5 mg cm^{-2}.

The membrane electrode assembly (MEA) was done by assembling electrodes and membrane in the single cell module with an applied torque of 4 Nm for every measurement.

Different MEAs (ie, electrodes with membranes of different thickness) were tested in a conventional configuration in order to study the performance of a DMFC using CS/PTA as proton conductor and to get information about the kinetics of the electrochemical reactions.

To evaluate the DMFC performance with CS/PTA membranes, 1 M methanol aqueous solution was fed to the anode with a flow rate of 2 mL min^{-1}, while humidified oxygen (99.5% purity) was fed to the cathode at 150 mL min^{-1} under 1 bar (Figure 1A). High purity graphite plates, with high electrical conductivity and high

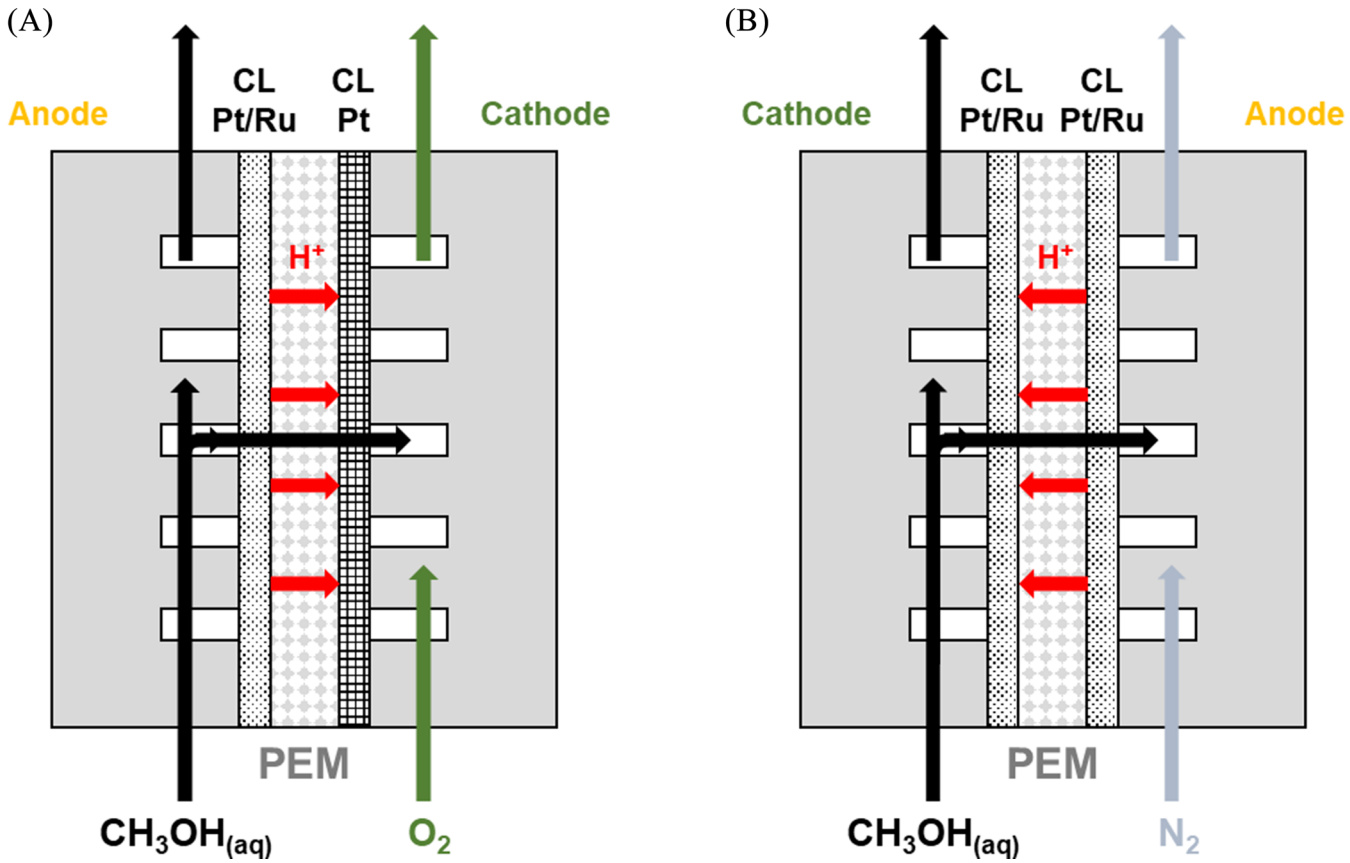

FIGURE 1 Schemes of the operating fuel cell modes. A, conventional fuel cell operation (methanol fed at the anode, oxygen fed at the cathode); B, crossover mode: methanol fed at the cathode and nitrogen fed at the anode [Colour figure can be viewed at wileyonlinelibrary.com]

thermal conductivity, were used for feeding methanol and oxygen to flow over the MEA (with serpentine flow channel). Teflon gaskets were placed between MEA and each of the graphite plates. Gold-plated plates were used as current collectors and are joined to the graphite plates.

EIS measurements were carried out by superimposing to the constant continuous potential a sinusoidal signal of amplitude 10 mV over the frequency range 100 kHz to 10 mHz. The EIS spectra were then fitted with ZSimpWin software.

All in-cell measurements were carried out at 70°C using a Parstat 4000 (Princeton Applied Research) and are referred to an active (apparent) area of 1 cm^2.

It is important to mention that the membranes are stable after the experimental tests and that they preserve their proton conductivity, as confirmed by recording further polarization curves.

2.5 | Methanol permeability study

Crossover mode (Figure 1B) was used to estimate methanol permeability of the membranes in an operating fuel cell by linear sweep voltammetry (LSV) and chronoamperometric measurements. At this aim, humidified N_2 was fed to the O_2 side of the cell, while methanol was fed to the other electrode. Potential was applied to the N_2 electrode so that, in this configuration, this electrode worked as anode and the only possible anodic process was the oxidation of methanol permeated from the other side of the cell. The electrode where methanol is directly fed worked as cathode (counter electrode) and as reference electrode (dynamic hydrogen electrode [DHE]), since H2 evolution occurred and it works as an ideally non-polarizable interface. During LSV measurements, electrode potential (N_2 side) was scanned from the OCP up to 0.85 V with a scan rate of 20 mV s^{-1} in order to measure a steady-state limiting current density, $j_{\lim}$, due to the electrooxidation of permeated methanol from the cathode to the anode side. The limiting current density can be expressed as follows[37]:

$$j_{\lim} = k_{dl}\frac{6Fc_mD_m}{d_m} \quad (2)$$

where k_{dl} is the electro-osmotic drag coefficient (protons transport through the membrane induced a solvent electro-osmotic transport), D_m is the methanol diffusivity in the membrane, and c_m is the methanol concentration in the membrane at the methanol feed/membrane interface. In order to estimate D_m, and c_m, chronoamperometric measurements were carried out to follow the current-time transients. During chronoamperometric measurements, the product ($jt^{1/2}$) reached a plateau value during the first seconds of the measurements, in the so-called Cottrell region (see Appendix A). By knowing the plateau value and j_{lim}, and by using k_{dt} and k_{dl} values derived by numerical simulation,[37] it is possible to estimate D_{m} according to the relationship:

$$D_m = \frac{k_{dt}^2}{k_{dl}^2}\frac{j_{lim}^2}{\left(j\sqrt{t}\right)^2}\frac{d_m^2}{\pi}. \quad (3)$$

3 | RESULTS AND DISCUSSION

3.1 | Membrane's morphology

SEM was employed to investigate membrane's morphology at the micro-scale. In Figure 2, the cross section of a 0.5 minute reticulated membrane is reported. From a closer inspection (see zoom in view in Figure 2), it is possible to note that so-formed membranes are compact and uniform in thickness, without the presence of any macro and microvoids in the membrane structure.

These characteristics are common to all the investigated membranes, as it is possible to see from the SEM images reported in Supplementary Material, where morphologies of membranes reticulated for different times are shown. With respect to our previous works,[32-35] we used a different porous medium impregnated of PTA for the reticulation step, that is, homemade anodic porous alumina (see anodizing conditions in Section 2.1) whose square pores had an area of ~1 μm^2 and pores were 40 μm long. This did not influence the good quality of the membranes synthesized by ionotropic gelation process.

3.2 | Membrane liquid uptake

Membrane's liquid uptake as a function of the reticulation time is reported in Figure 3. It is important to recall that membrane thickness was efficiently controlled through the reticulation time, that is, contact time between CS/acetic acid solution and porous medium impregnated of PTA.[32-34] Using deionized water during the test, the liquid uptake is very high for the lowest thickness (ie, 17 ± 4 μm, see Supplementary Material), significantly higher than that of Nafion membrane.[38] Water uptake drastically decreases by increasing the membrane thickness becoming almost constant (~70%) for thicker layers. Notably, liquid uptake does not change when 1 M methanol aqueous solution is used during the test. This result leads to the conclusion that the CS-PTA

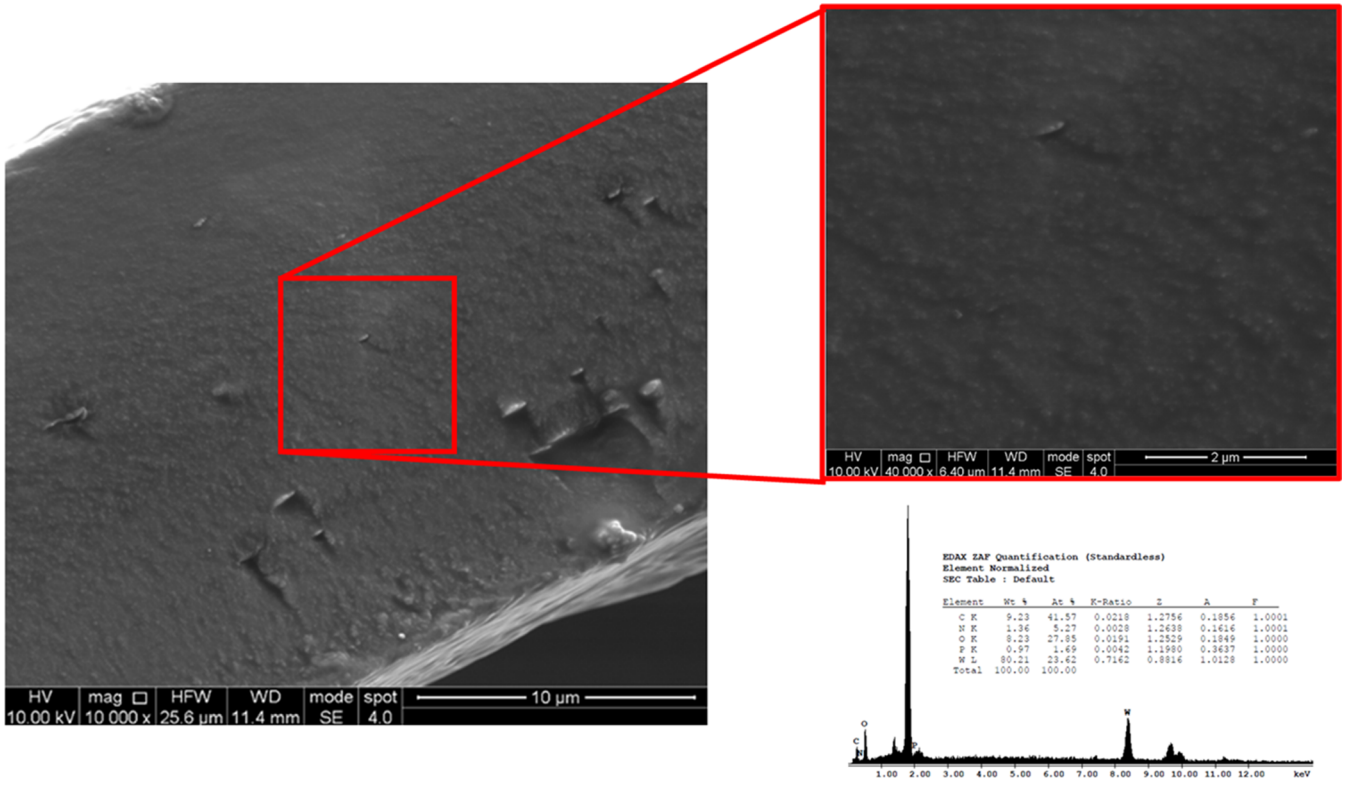

FIGURE 2 SEM cross-sectional micrograph of a CS/PTA membrane after a reticulation time of 0.5 minute and a functionalization time of 24 hours. Inset: elemental composition of the membrane obtained using EDS analysis. CS, chitosan; EDS, Energy Dispersive X-ray Spectrometry; PTA, phosphotungstic acid; SEM, scanning electron microscopy [Colour figure can be viewed at wileyonlinelibrary.com]

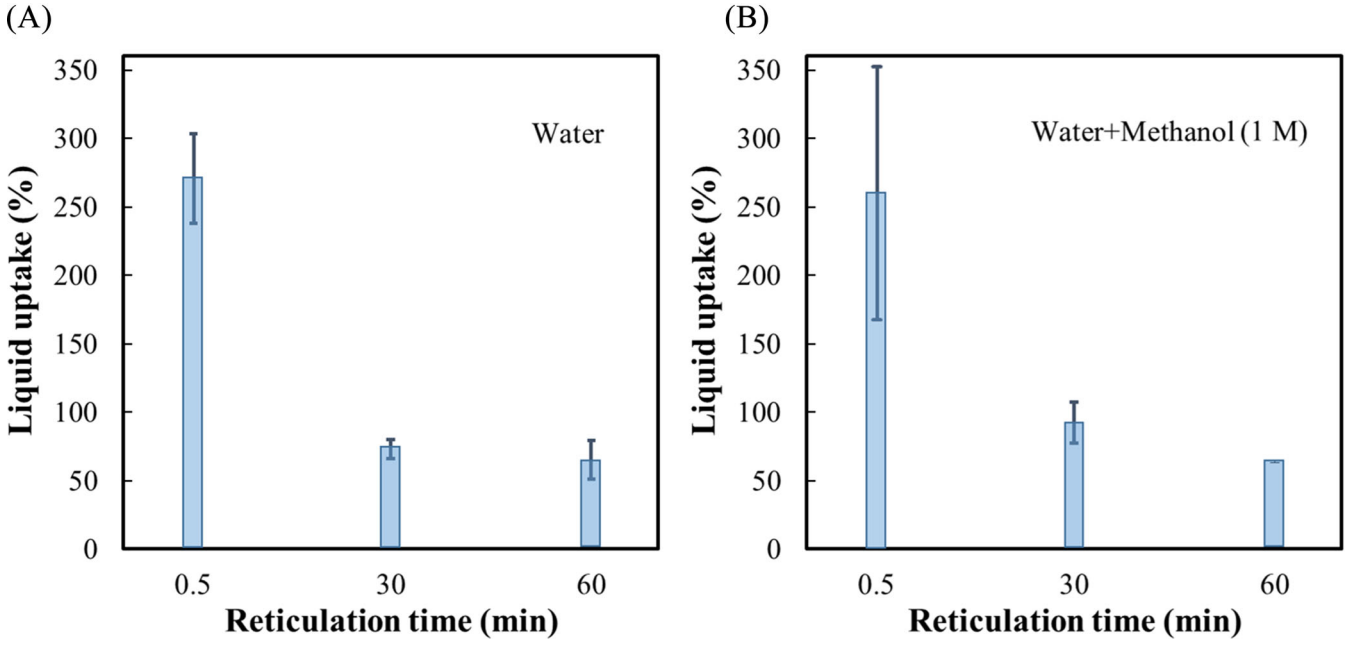

FIGURE 3 Liquid uptake values as a function of reticulation time by using, A, distilled water and, B, a methanol aqueous solution (1 M) [Colour figure can be viewed at wileyonlinelibrary.com]

membranes do not show a high level of "methanol-philicity."

Knowing the liquid uptake, it was also possible to estimate the membrane's porosity, ε, according to the following relationship[37]:

$$\varepsilon = \frac{(W_{wet} - W_{dry})\rho_{dry}}{(W_{wet} - W_{dry})\rho_{dry} + W_{dry}\rho_{sol}} \quad (4)$$

where ρ_{dry} and ρ_{sol} are membrane and methanol solution densities, respectively. Membrane porosity decreases by increasing the membrane thickness, from 0.77 to 0.53 reaching a value comparable to that estimated for Nafion 117.[37] This dependence agrees with the trend of the liquid uptake suggesting that the membrane thickening during the reticulation process is accompanied by a change in the structure of the polymer, namely by an increase of the cross linking among the chitosan chains.

Membrane's water uptake is a key factor, since water is necessary to grant a good proton conductivity.[1,39,40] However, a high water uptake like that measured for the thinnest membrane can lead to a high methanol crossover, poor mechanical stability (especially at high temperature) and a possible flooding of the cell with detrimental effect on the performances.

3.3 | Fuel cell performances

Figure 4A shows polarization and power density curves recorded with a membrane reticulated for 30 minutes at different operating temperatures (ie, 30, 50, and 70°C), while in Figure 4B, a comparison between polarization and power density curves recorded by using a thin membrane (ie, reticulation time 30 seconds) and a thick membrane (ie, reticulation time 30 minutes) is reported. All the measurements referred to membranes functionalized in PTA aqueous solution for 24 hours.

The recorded open-circuit voltages (OCVs), regardless operating temperature, are lower than thermodynamic cell electromotive force (*emf*) of 1.21 V that is a function of the molar Gibbs free energy of formation of products and reactants involved in the overall reaction (see Equation 6) through the following relationship[41]:

$$\text{emf} = -\frac{\Delta G}{zF} \quad (5)$$

where ΔG is the change in the Gibb's free energy related to the overall cell reaction, z is the number of electrons transferred per mole of fuel, and F is the Faraday constant (96 480 C). For a DMFC, the overall cell reaction is[42]:

$$CH_3OH + 3/2\,O_2 \rightarrow 2H_2O + CO_2 \quad (6)$$

where the number of electrons (ie, z) produced by the methanol electrooxidation, carried out at the anode, is 6. OCV values lower than *emf* due to the methanol crossover, across the polymer membrane, from the anodic to cathodic compartment with consequent depolarization of the cathode. This phenomenon is more significant for thin membranes (lower OCV), while for thicker membranes, the OCV is comparable to that measured using Nafion and Nafion-based polymeric electrolyte.[38,43-45]

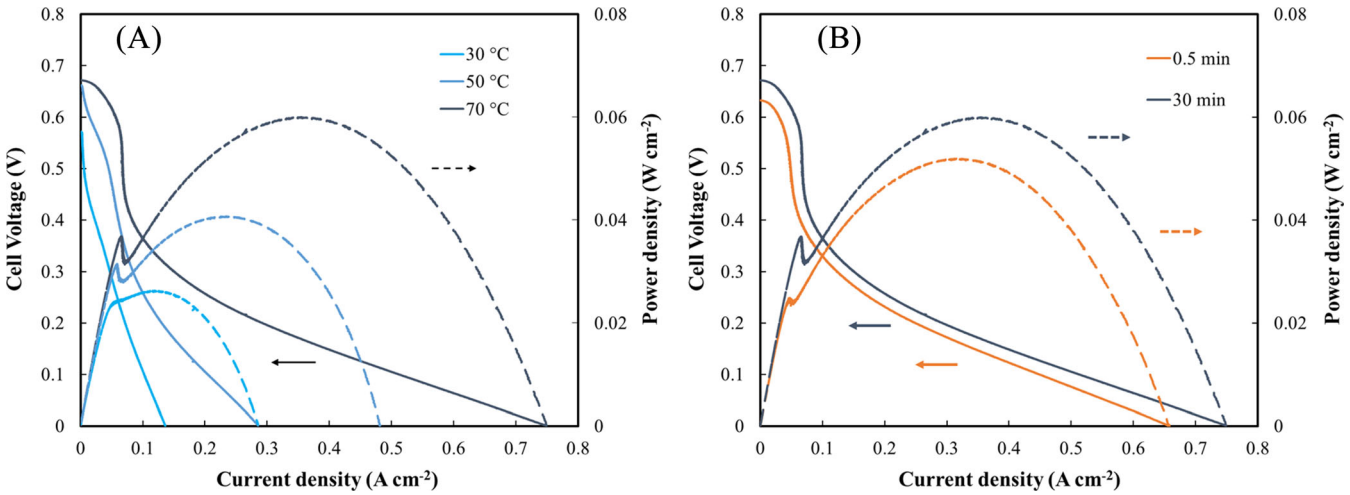

FIGURE 4 Polarization and power density curves as a function of current density curves recorded using, A, 30 minutes reticulated membrane at different operating temperature (30, 50, and 70°C) and, B, 0.5 minute and 30 minutes reticulated membranes, at 70°C [Colour figure can be viewed at wileyonlinelibrary.com]

It is noteworthy to mention that by increasing the operating temperature, enhanced performances (in terms of OCV, membrane resistance and power density peak values) were obtained, with the best performances got at 70°C (Figure 4A). Therefore, as displayed in Figure 4B, CS/HPA membranes reticulated for 30 minutes work efficiently as proton conductors in DMFC allowing to get power density of 60 mW cm^{-2} at 70°C with a Pt load of 0.5 mg cm^{-2} at the cathode (ie, for O_2 reduction) and a Pt-Ru load of 3 mg cm^{-2} at the anode (ie, for methanol oxidation). Comparable performances were obtained using membranes reticulated for 60 minutes, while for short reticulation time (ie, 0.5 minute; Figure 4B), worst and not reproducible performances were obtained. As a general result, it is worth noting that thin membranes are not appropriate for this application, while thicker CS-PTA composite membranes (ie, those reticulated for 30-60 minutes) show performances comparable to those recorded using recast Nafion[38] in methanol-fed fuel cells, in terms of OCV and peak power density, and are better or comparable than those related to other CS-based membranes for acidic DMFCs,[29] usually studied with a higher methanol concentration (eg, 2 M) and/or with a higher Pt loading.

Two different zones are visible in the polarization curve: the activation region (between OCV and ~0.3 V), where the kinetic losses are due to the electrochemical reaction, and the ohmic region where the potential drop is mainly due to the resistance of the membrane. The shake shown in the activation region of polarization curve is supposed to be due to a slow desorption of intermediate species produced by methanol oxidation at the anode at low overvoltage values. From the slope of the ohmic region of the polarization curve, it is possible to estimate a membrane resistance, R_m, of ~0.44 Ω cm^2, which is comparable to that estimated for H_2-fed low temperature fuel cell with CS/HPA membranes and significantly lower with respect to that estimated for Nafion membranes in DMFC.[38] From membrane resistance value, it is possible to estimate the membrane proton conductivity, σ, as follows:

$$\sigma = \frac{d_m}{R_m A} \tag{7}$$

where d_m is the membrane thickness (ie, 52 μm). This leads to a membrane proton conductivity value of 12.4 mS cm^{-1}, comparable or higher than other CS-based polymer electrolyte membranes.[46]

Notably, the potential loss in the activation region is very high indicating that the electrooxidation of methanol is a sluggish reaction even using Pt/Ru catalysts. This statement is also supported by the EIS spectra recorded at constant potential in the activation region (ie, 0.5 V), displayed in Figure 5 in the Nyquist representation.

Two depressed semicircles are clearly visible suggesting a contribution of the charge transfer resistance of both half-cell reactions (methanol oxidation and oxygen reduction) to the overall impedance. These experimental findings suggest that the performance of the DMFC is strongly affected by the methanol crossover and by the overpotential necessary to activate the CH_3OH oxidation reaction. Moreover, it is noteworthy to mention that Nyquist diagram of EIS spectrum is also characterized by the beginning of an inductive loop in the low frequency domain. This impedance response suggests that the kinetics of electrochemical reaction at the anode is also dependent on surface coverage, implying the crucial role of absorbing species at the electrode.

To understand in which extent these factors affect the cell performance, we considered the MOR, which follows a rather complex mechanism involving several chemical and electrochemical steps, simplified according to the two-step model described by the following reactions:

$$CH3OH \xrightarrow{k_1} CO_{ads} + 4H+ + 4e^- \tag{8a}$$

$$CO_{ads} + H2O \xrightarrow{k_2} CO2 + 2H+ + 2e^- \tag{8b}$$

where k_1 and k_2 are the rate constants of the two involved reactions. The first step is the methanol oxidation to a reaction intermediate, CO_{ads}, while the second step is the oxidation of these adsorbed species to CO_2. The bifunctional mechanism operating during methanol electrooxidation on bimetallic catalyst, as that employed in this work (ie, a Pt/Ru catalyst), foresees that methanol is preferentially adsorbed on Pt sites, while OH comes from water dissociation on Ru sites. If we assume that only one intermediate (ie, CO_{ads}) is involved in the overall MOR, the Faradaic current, j_F, across the electrode can be expressed as the sum of two contributions, that is,

$$j_F = j_1 + j_2 \tag{9}$$

where

$$j_1 = k_1 (1 - \gamma_{CO}) \exp(b_1 E) \tag{10a}$$

$$j_2 = k_2 \gamma_{CO} \exp(b_2 E) \tag{10b}$$

and γ_{CO} represents the fractional surface coverage by intermediate CO_{ads}, b_1 and b_2 the Tafel slope for the reactions reported with Equations (8a) and (8b), and E the imposed continuous potential (ie, overpotential). Therefore, the net Faradaic current density is a function of

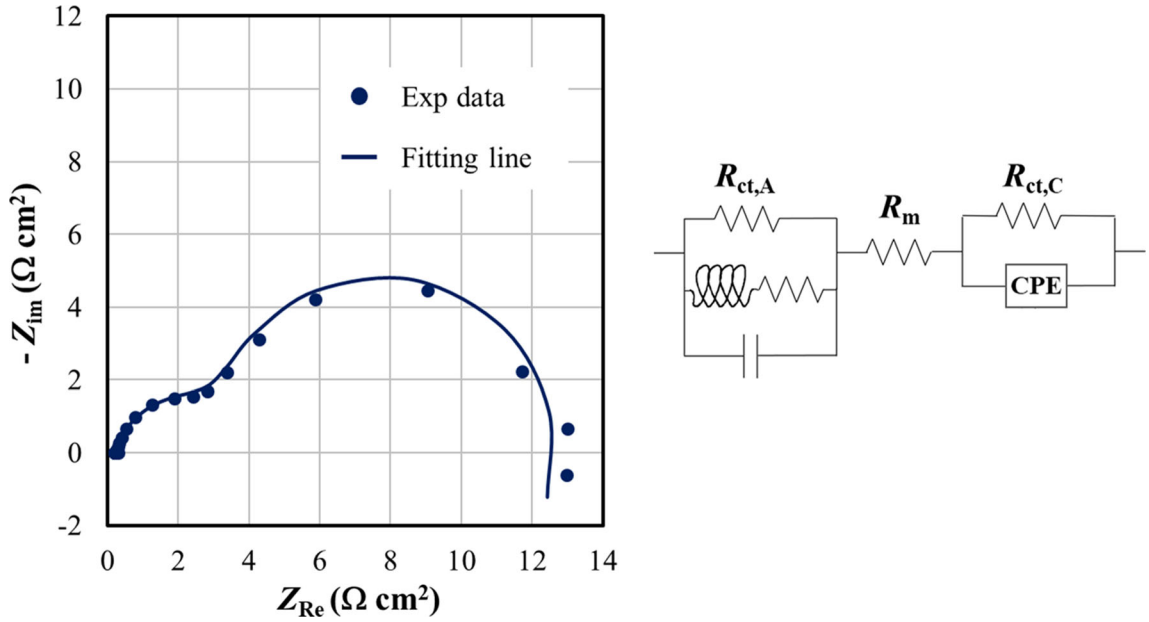

FIGURE 5 EIS spectrum in Nyquist representation recorded at 0.5 V employing a 30 minutes reticulated membrane at 70°C. EIS, electrochemical impedance spectroscopy [Colour figure can be viewed at wileyonlinelibrary.com]

both γ_{CO} and E, thus polarization curves are not sufficient to study the kinetics of CH_3OH oxidation in the cell conditions, and it is necessary to record EIS spectra. When an ac signal $\tilde{E}$ of frequency ω is superimposed to the continuous polarization, the corresponding oscillating current, $\tilde{j}$, can be expressed as:

$$\tilde{j} = Y\tilde{E} = Z^{-1}\tilde{E} \tag{11}$$

where Y is the admittance for methanol oxidation, that is, the reciprocal of the impedance, Z. As reported in detail in Appendix B, Y is given by the following equation:

$$Y = \frac{1}{R_{ct}} + \frac{A}{B + j\omega} \tag{12}$$

corresponding to an equivalent circuit which is function of the A value. More specifically, when $A > 0$, the electrical equivalent circuit providing the impedance response for the MOR is reported in the inset of Figure 5. In particular, a charge transfer resistance, $R_{ct,A}$, is in parallel with an inductance in series with a resistance, with values of $1/A$ and A/B, respectively. In order to take into account the presence of the double layer capacitance, the element C_A has to be inserted in parallel with the circuit described above. When $A > 0$, k_1 results have to be comparable with k_2, thus it is not possible to clearly identify a rate-determining step in reactions (8a) and (8b).[47] This agrees with the idea that HPAs facilitate the oxidative removal of CO_{ads} poisoning species for methanol oxidation, enhancing the anode kinetics.[30,31] To model the behavior of the entire fuel cell system, R_m in series with a resistance, $R_{ct,C}$ in parallel with a constant phase element, Q_C, were added to the electrical equivalent circuit, accounting for the ionic membrane resistance and for the electrochemical behavior of the cathode. From the fitting of the EIS spectrum, $R_{ct,A}$ (8.9 Ω cm^2) resulted to be three times higher than $R_{ct,C}$ (2.9 Ω cm^2), confirming that the methanol electrooxidation is a sluggish reaction, even slower than oxygen reduction reaction. However, the estimated charge transfer resistance related to MOR is lower than most of $R_{ct,A}$ reported in literature, although the latter are often estimated ex-situ, using a three-electrode configuration in aqueous methanol solution.[47-50]

3.4 | Methanol permeability

To study methanol permeability under the cell operating conditions (ie, membrane inside the MEA at 70°C with flowing streams of reagents), we followed the approach described in the work of Ren et al[37] and Majidi et al,[51] as described in Section 2. Thus, electrochemical tests were carried out using the fuel cell in the crossover configuration mode (Figure 1B). LSVs were recorded in order to determine the mass-transfer-controlled potential region and the corresponding limiting current for the oxidation of methanol at Pt/Ru catalyst layer in the N_2 side (Figure 6). During the measurements, the recorded anodic current density is due to methanol oxidation and is directly proportional to the content of methanol that

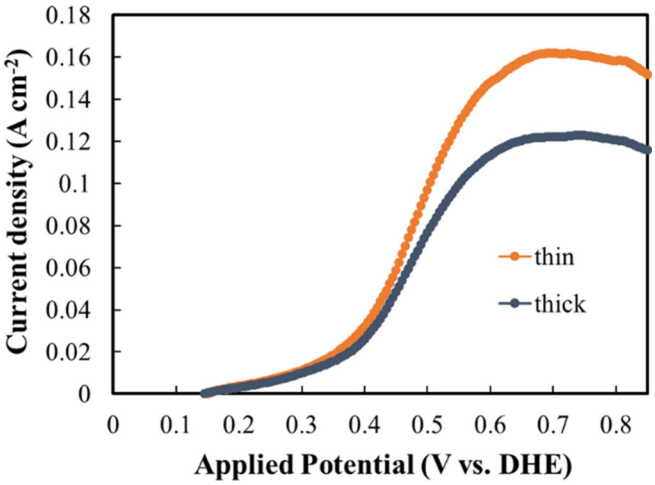

FIGURE 6 LSV curves of thin (reticulated for 0.5 minute) and thick (reticulated for 60 minutes) membranes to evaluate methanol diffusivity, recorded in crossover mode at 70°C. LSV, linear sweep voltammetry [Colour figure can be viewed at wileyonlinelibrary.com]

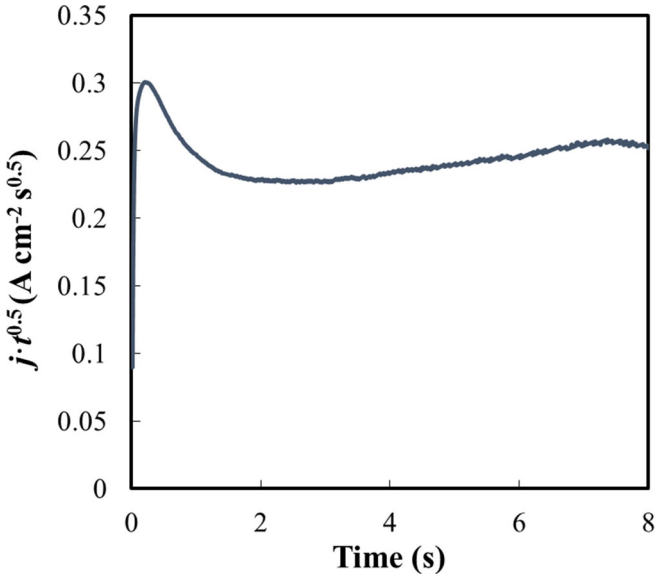

FIGURE 7 Cottrell plot of current transient recorded at 0.85 V in crossover mode, employing a thick (reticulated for 60 minutes) membrane, at 70°C [Colour figure can be viewed at wileyonlinelibrary.com]

crossed the membrane (permeate) and reacted at the Pt/Ru catalyst in an inert atmosphere, such as that created by humidified N_2. The cathodic process occurring at methanol feeding electrode was H_2 evolution on the same Pt/Ru catalyst, that is, an electrochemical reaction which has very fast kinetics on noble metals.

According to Ren et al,[37] the main factors influencing the methanol permeation rate across a polymeric membrane in a DMFC are the methanol concentration drop across the carbon cloth backing, the membrane hydration level and the CH_3OH convective flux driven by electro-osmotic drag associated to the proton transport inside the composite CS/PTA membrane. Since the water present on both the electrodes of the DMFC is enough to keep the membrane fully hydrated, and since the carbon cloth backing has a very porous structure, the key factor affecting the methanol permeation is the convective transport due to the electro-osmotic drag of ionic current carried by protons. The latter phenomenon must be taken into account to properly assess the membrane diffusivity.

During the LSV, limiting current densities (j_{lim}) of 150 and 117 mA cm^{-2} are reached for thin (ie, reticulated for 0.5 minute) and thick membranes (ie, reticulated for 30 and 60 minutes), respectively. These j_{lim} values are comparable or even lower than the values estimated with the same experimental approach using recast Nafion membranes.[38] It is important to say that the limiting current density is directly dependent on the amount of methanol passing through the membrane, thus the higher is j_{lim}, the higher is the methanol crossover across composite CS/PTA membranes. The result shown in Figure 6 well agrees with the results reported in Sections 3.2 and 3.3: thin membranes have higher liquid uptake and porosity with respect to thick membranes, leading to worse performances in the single fuel cell module derived from a too high methanol crossover.

Figure 7 shows the ($jt^{1/2}$) vs t plot, recorded using a thick membrane (reticulated for 60 minutes) during the chronoamperometric measurement at 0.85 V/DHE, that is, under mass transfer kinetic control.

The product ($jt^{1/2}$) reached a plateau value during the first seconds of the measurements, in the so-called Cottrell region (see Appendix A). By knowing the plateau value and j_{lim}, and by using k_{dt} and k_{dl} values derived by numerical simulation,[37] it is possible to estimate D_m according to Equation (3). Consequently, it is straightforward to calculate c_m from Equation (2) of value of 0.44 M and $D_m = 3.6 \times 10^{-6}$ cm^2 s^{-1}. Finally, it was possible to calculate the concentration profiles inside the CS/PTA membranes at different times according the following equation[41]:

$$c(x,t) = c_m erf\left[\frac{x}{2\sqrt{(D_m t)}}\right]. \quad (13)$$

and $c(x,t)/c_m$ plot is shown in Figure 8.

D_m value is one order of magnitude lower than that reported for methanol in aqueous solution (1.6×10^{-5} cm^2 s^{-1}),[52] supposed to be due to a high level of tortuosity of the CS/PTA composite membranes. It is also noteworthy to mention that the diffusivity estimated

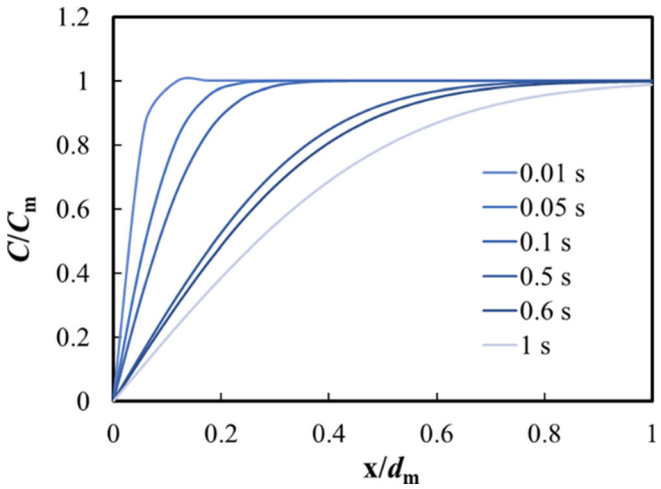

FIGURE 8 Concentration profile inside the CS/PTA membrane at different times, estimated through Equation (13). CS, chitosan; PTA, phosphotungstic acid [Colour figure can be viewed at wileyonlinelibrary.com]

by this procedure is comparable to those estimated for Nafion and different Nafion-based membranes.[38,53]

4 | CONCLUSIONS

Composite CS/PTA not perfluorinated membranes were prepared by ionotropic gelation on an inert porous medium releasing the HPA and functionalized in the same HPA. These membranes are compact and uniform and show a high liquid uptake but a low level of methanol-philicity. Then, they were successfully tested as proton conductors in DMFCs. The polarization curves show that it is possible to get a really promising peak power density of 60 mW cm^{-2} at 70°C with a low methanol concentration (1 M) and low catalysts loadings at the electrodes, with a quite low membrane resistance (lower than that measured for Nafion) leading to a proton conductivity of ~12 mS cm^{-1}.

The analysis of the polarization curves revealed that crossover phenomena (as indicated by the OCV lower than the reversible cell potential) and the high activation losses for methanol oxidation limit the performance of the cell. *In-cell* tests carried out allowed to estimate a diffusivity in the order of 10^{-6} cm^2 s^{-1}, lower than permeabilities estimated for many CS-based membranes used as polymer electrolytes and comparable to that estimated for Nafion and different Nafion-based membranes.

These promising experimental results suggest that CS/PTA proton conductors are good candidate for replacing perfluorinated membranes, even if other efforts are necessary to further improve their stability.

ACKNOWLEDGEMENTS

Dr. Irene Gatto (CNR ITAE Institute for Advanced Energy Technologies "N. Giordano," Italy) is gratefully acknowledged for providing Pt and Pt/Ru electrodes. A. Z. acknowledges support from the Italian Ministry of Education, University and Research (MIUR) within the program PON R&I 2014-2020—Attraction and International Mobility (AIM)—project no. AIM1845825-3.

ORCID

Francesco Di Franco https://orcid.org/0000-0002-5722-2881

REFERENCES

1. Kreuer KD. On the development of proton conducting polymer membranes for hydrogen and methanol fuel cells. *J Memb Sci*. 2001;185:29-39.
2. Lamy C, Lima A, LeRhun V, Delime F, Coutanceau C, Léger JM. Recent advances in the development of direct alcohol fuel cells (DAFC). *J Power Sources*. 2002;105:283-296.
3. Ong BC, Kamarudin SK, Basri S. Direct liquid fuel cells: a review. *Int J Hydrog Energy*. 2017;42:10142-10157.
4. Wu QX, Zhao TS, Chen R, An L. A sandwich structured membrane for direct methanol fuel cells operating with neat methanol. *Appl Energy*. 2013;106:301-306.
5. Neburchilov V, Martin J, Wang H, Zhang J. A review of polymer electrolyte membranes for direct methanol fuel cells. *J Power Sources*. 2007;169:221-238.
6. Lufrano F, Baglio V, Staiti P, Antonucci V, Arico' AS. Performance analysis of polymer electrolyte membranes for direct methanol fuel cells. *J Power Sources*. 2013;243:519-534.
7. Lin HL, Wang SH. Nafion/poly(vinyl alcohol) nano-fiber composite and Nafion/poly(vinyl alcohol) blend membranes for direct methanol fuel cells. *J Memb Sci*. 2014;452:253-262.
8. Mondal S, Soam S, Kundu PP. Reduction of methanol crossover and improved electrical efficiency in direct methanol fuel cell by the formation of a thin layer on Nafion 117 membrane: effect of dip-coating of a blend of sulphonated PVdF-co-HFP and PBI. *J Memb Sci*. 2015;474:140-147.
9. Hu M, Zhang B, Chen J, Xu M, Liu D, Wang L. Cross-linked polymer electrolyte membrane based on a highly branched sulfonated polyimide with improved electrochemical properties for fuel cell applications. *Int J Energy Res*. 2019;43:8753-8764.
10. Liu G, Wang M, Wang Y, Tian Z, Wang X. A novel anode catalyst layer with multilayer and pore structure for improving the performance of a direct methanol fuel cell. *Int J Energy Res*. 2013;37:1313-1317.
11. Haghnegahdar S, Noroozifar M. Palladized dysprosium fluoride nanorods as a new performance catalyst in direct methanol fuel cell. *Int J Energy Res*. 2019;43:4701-4714.
12. Wu D, Xu T, Wu L, Wu Y. Hybrid acid–base polymer membranes prepared for application in fuel cells. *J Power Sources*. 2009;186:286-292.
13. Zhang Y, Cai W, Si F, et al. A modified Nafion membrane with extremely low methanol permeability via surface coating of sulfonated organic silica. *Chem Commun*. 2012;48:2870-2872.

14. Awang N, Ismail AF, Jaafar J, et al. Functionalization of polymeric materials as a high performance membrane for direct methanol fuel cell: a review. *React Funct Polym*. 2015;86:248-258.
15. Bhattad SS, Mahanwar PA. Functionalized and electrospun polymeric materials as high-performance membranes for direct methanol fuel cell: A Review. *J Membr Sci Res*. 2017;3:240-247.
16. Yadav V, Rajput A, Rathod NH, Kulshrestha V. Enhancement in proton conductivity and methanol cross-over resistance by sulfonated boron nitride composite sulfonated poly (ether ether ketone) proton exchange membrane. *Int J Hydrog Energy*. 2020; 45:17017-17028.
17. Cui F, Wang W, Liu C, Chen X, Li N. Carbon nanocomposites self-assembly UiO-66-doped chitosan proton exchange membrane with enhanced proton conductivity. *Int J Energy Res*. 2020;44:4426-4437.
18. Mauritz KA, Moore RB. State of understanding of Nafion. *Chem Rev*. 2004;104:4535-4585.
19. Rinaudo M. Chitin and chitosan: properties and applications. *Prog Polym Sci*. 2006;31:603-632.
20. Muthumeenal A, Neelakandan S, Kanagaraj P, Nagendran A. Synthesis and properties of novel proton exchange membranes based on sulfonated polyethersulfone and N-phthaloyl chitosan blends for DMFC applications. *Renew Energy*. 2016;86:922-929.
21. Nur H, Muhammad M, Hamid A, Herry P, Dwilaksita A, Zubaida FR. Preliminary study of ABS/chitosan blend polymer for DMFC membranes. *Mater Sci Forum*. 2019;961:23-29.
22. Hanna ANR, Loh KS, Wong WY, et al. Review of chitosan-based polymers as proton exchange membranes and roles of chitosan-supported ionic liquids. *Int J Mol Sci*. 2020;21:632.
23. Di Franco F, Zaffora A, Burgio G, Santamaria M. Performance of H2-fed fuel cell with chitosan/silicotungstic acid membrane as proton conductor. *J Appl Electrochem*. 2020;50:333-341.
24. Mohanapriya S, Bhat SD, Sahu AK, Pitchumani S, Sridhar P, Shukla AK. A new mixed-matrix membrane for DMFCs. *Energy Environ Sci*. 2009;2:1210-1216.
25. Amirinejad M, Madaeni SS, Navarra MA, Rafiee E, Scrosati B. Solvent-free nanocomposite proton-conducting membranes composed of cesium salt of phosphotungstic acid doped PVDF–CTFE/PEO blend. *Ionics*. 2010;16:681-687.
26. Madaeni SS, Amirinejad S, Amirinejad M. Phosphotungstic acid doped poly(vinyl alcohol)/poly(ether sulfone) blend composite membranes for direct methanol fuel cells. *J Memb Sci*. 2011;380:132-137.
27. Kourasi M, Wills RGA, Shah AA, Walsh FC. Heteropolyacids for fuel cell applications. *Electrochim Acta*. 2014;127:454-466.
28. Cui Z, Liu C, Lu T, Xing W. Polyelectrolyte complexes of chitosan and phosphotungstic acid as proton-conducting membranes for direct methanol fuel cells. *J Power Sources*. 2007;167:94-99.
29. Wu Q, Wang H, Lu S, Xu X, Liang D, Xiang Y. Novel methanol-blocking proton exchange membrane achieved via self-anchoring phosphotungstic acid into chitosan membrane with submicro-pores. *J Membr Sci*. 2016;500:203-210.
30. Cui Z, Li CM, Jiang SP. PtRu catalysts supported on heteropolyacid and chitosan functionalized carbon nanotubes for methanol oxidation reaction of fuel cells. *Phys Chem Chem Phys*. 2011;13:16349-16357.
31. Wang D, Lu S, Xiang Y, Jiang SP. Self-assembly of HPW on Pt/C nanoparticles with enhanced electrocatalysis activity for fuel cell applications. *Appl Catal B Environ*. 2011;103:311-317.
32. Santamaria M, Pecoraro CM, Di Quarto F, Bocchetta P. Chitosan–phosphotungstic acid complex as membranes for low temperature H2–O2 fuel cell. *J Power Sources*. 2015;276: 189-194.
33. Pecoraro CM, Santamaria M, Bocchetta P, Di Quarto F. Influence of synthesis conditions on the performance of chitosan–Heteropolyacid complexes as membranes for low temperature H2–O2 fuel cell. *Int J Hydrog Energy*. 2015;40:14616-14626.
34. Santamaria M, Pecoraro CM, Di Franco F, Di Quarto F, Gatto I, Saccà A. Improvement in the performance of low temperature H2–O2 fuel cell with chitosan–phosphotungstic acid composite membranes. *Int J Hydrog Energy*. 2016;41:5389-5395.
35. Santamaria M, Pecoraro CM, Di Franco F, Di Quarto F. Phosphomolybdic acid and mixed phosphotungstic/phosphomolybdic acid chitosan membranes as polymer electrolyte for H_2/O_2 fuel cells. *Int J Hydrog Energy*. 2017;42:6211-6219.
36. Gatto I, Saccà A, Carbone A, Pedicini R, Urbani F, Passalacqua E. CO-tolerant electrodes developed with PhosphoMolybdic acid for polymer electrolyte fuel cell (PEFCs) application. *J Power Sources*. 2007;171:540-545.
37. Ren X, Springer TE, Zawodzinski TA, Gottesfeld S. Methanol transport through nation membranes. Electro-osmotic drag effects on potential step measurements. *J Electrochem Soc*. 2000;147:466-474.
38. Ru C, Gu Y, Duan Y, Zhao C, Na H. Enhancement in proton conductivity and methanol resistance of Nafion membrane induced by blending sulfonated poly(arylene ether ketones) for direct methanol fuel cells. *J Memb Sci*. 2019;573:439-447.
39. Izquierdo-Gil MA, Barragán VM, Villaluenga JPG, Godino MP. Water uptake and salt transport through Nafion cation-exchange membranes with different thicknesses. *Chem Eng Sci*. 2012;72:1-9.
40. Zawodzinski TA, Derouin C, Radzinski S, et al. Water uptake by and transport through Nafion® 117 membranes. *J Electrochem Soc*. 1993;140:1041-1047.
41. Bard AJ, Faulkner LR. Potentials and Thermodynamic of cells. *Electrochemical Methods: Fundamentals and Applications*. New Yorke Chichester • Weinheim Brisbane e Singapore e Toronto: John Wiley & Sons; 2001.
42. Ince AC, Karaoglan MU, Glüsen A, Colpan CO, Müller M, Stolten D. Semiempirical thermodynamic modeling of a direct methanol fuel cell system. *Int J Energy Res*. 2019;43:3601-3615.
43. Lin HL, Yu TL, Huang LN, Chen LC, Shen KS, Bin JG. Nafion/PTFE composite membranes for direct methanol fuel cell applications. *J Power Sources*. 2005;150:11-19.
44. Chen LC, Yu TL, Lin HL, Yeh SH. Nafion/PTFE and zirconium phosphate modified Nafion/PTFE composite membranes for direct methanol fuel cells. *J Memb Sci*. 2008;307:10-20.
45. Wang SH, Lin HL. Poly(vinylidene fluoride-co-hexafluoropropylene)/polybenzimidazole blend nanofiber supported Nafion membranes for direct methanol fuel cells. *J Power Sources*. 2014;257:254-263.
46. Lupatini KN, Schaffer JV, Machado B, et al. Development of chitosan membranes as a potential PEMFC electrolyte. *J Polym Environ*. 2018;26:2964-2972.
47. Wu G, Li L, Xu BQ. Effect of electrochemical polarization of PtRu/C catalysts on methanol electrooxidation. *Electrochim Acta*. 2004;50:1-10.
48. Wang Z-B, Zuo P-J, Yin G-P. Investigations of compositions and performance of PtRuMo/C ternary catalysts for methanol electrooxidation. *Fuel Cells*. 2009;9:106-113.
49. Zhiani M, Jalili J, Rezaei B, Taghiabadi MM. Methanol electrooxidation on synthesized PtRu nanocatalyst supported on acetylene black in half cell and in direct methanol fuel cell. *Int J Hydrog Energy*. 2013;38:5419-5424.

50. Preda L, Kondo T, Spataru T, et al. Enhanced activity for methanol oxidation of platinum particles supported on iridium oxide modified boron-doped diamond powder. *Chem Electro Chem*. 2017;4:1908-1915.
51. Majidi P, Altarawneh RM, Ryan NDW, Pickup PG. Determination of the efficiency of methanol oxidation in a direct methanol fuel cell. *Electrochim Acta*. 2016;199:210-217.
52. Verbrugge MW. Methanol diffusion in perfluorinated ion-exchange membranes. *J Electrochem Soc*. 1989;136:417-423.
53. Rambabu G, Nagaraju N, Bhat SD. Functionalized fullerene embedded in Nafion matrix: a modified composite membrane electrolyte for direct methanol fuel cells. *Chem Eng J*. 2016;306:43-52.
54. Orazem ME, Tribollet B. Kinetic models. *Electrochemical Impedance Spectroscopy*. Hoboken, NJ: John Wiley & Sons; 2008.

SUPPORTING INFORMATION

Additional supporting information may be found online in the Supporting Information section at the end of this article.

How to cite this article: Zaffora A, Di Franco F, Gradino E, Santamaria M. Methanol and proton transport through chitosan-phosphotungstic acid membranes for direct methanol fuel cell. *Int J Energy Res*. 2020;44:11550–11563. https://doi.org/10.1002/er.5777

APPENDIX A

For the study of membrane's methanol permeability, we coupled LSV and chronoamperometric measurements. The latter ones were carried out at a suitable electrode potential, that is, at that potential where (permeated) methanol electrooxidation is under mass transfer kinetic control. Under this operating condition, the dependence of current density on time is described by the Cottrell equation[41]

$$j(t) = k_{dt}\frac{nFc_m\sqrt{D_m}}{\sqrt{\pi t}} \tag{A.1}$$

where F is the Faraday constant, n is the number of exchanged electrons, and k_{dt} is the electro-osmotic drag coefficient accounting for the electro-osmotic drag effect during the current transient.[37] Cottrell equation is derived solving the second Fick's law for a planar electrode and assuming a semi-infinite diffusion model, homogeneity of the methanol concentration inside the membrane before the polarization ($t = 0$), and methanol concentration equal to 0 at the electrode surface during the experiment ($t > 0$).

APPENDIX B

MOR comprises numerous chemical and electrochemical steps but can be simplified with the two-step model described by Equations (8a) and (8b). These reactions involve the formation of CO_{ads} from the oxidation of methanol, and the stripping of CO_{ads} with the final formation of CO_2. It is clear, from Equations (10a) and (10b), that the net Faradaic current of the methanol oxidation process is a function of CO surface coverage and electrode potential. The time variation of the surface coverage of the intermediate CO_{ads}, γ_{CO}, can be expressed by the following relationship[54]:

$$\Gamma\frac{\gamma_{CO}}{dt} = \frac{j_1}{F} - \frac{j_2}{F} \tag{B.1}$$

being Γ the maximum surface concentration of CO_{ads}. Under steady-state condition, $d\gamma_{CO}/dt = 0$ and, thus, $j_1 = j_2$. By using Equations (10a) and (10b), the expression of the steady state γ_{CO} is given by:

$$\gamma_{CO} = \frac{K_1\exp(b_1E)}{K_1\exp(b_1E) + K_2\exp(b_2E)}. \tag{B.2}$$

From Equation (B.2), it is possible to note that if reaction (8a) is much faster than reaction (8b), then $\gamma_{CO} \rightarrow 1$. On the contrary, if reaction (8a) is much slower than reaction (8b), then $\gamma_{CO} \rightarrow 0$. The expression for the total steady state current density is given by

$$j_F = j_1 + j_2 = \frac{2K_1\exp(b_1E)K_2\exp(b_2E)}{K_1\exp(b_1E) + K_2\exp(b_2E)}. \tag{B.3}$$

The oscillating component of the current density for the reactions (8a) and (8b) is given by

$$\tilde{j}_1 = {R_{ct,1}}^{-1}\tilde{E} - K_1\exp(b_1E)\tilde{\gamma}_{CO} \tag{B.4}$$

and

$$\tilde{j}_2 = {R_{ct,2}}^{-1}\tilde{E} + K_2\exp(b_2E)\tilde{\gamma}_{CO} \tag{B.5}$$

being the charge transfer resistances R_{ct} defined by:

$$R_{ct,1} = [K_1(1-\gamma_{CO})b_1\exp(b_1E)]^{-1} \tag{B.6}$$

and

$$R_{ct,2} = [K_2\gamma_{CO}b_2\exp(b_2E)]^{-1}. \tag{B.7}$$

According to Equation (B.1), the oscillating component of the surface coverage of CO_{ads} can be expressed as follows:

$$\begin{aligned}\Gamma Fj\omega\tilde{\gamma}_{CO} = &\left({R_{ct,1}}^{-1} - {R_{ct,2}}^{-1}\right)\tilde{E} \\ &- (K_1\exp(b_1E) + K_2\exp(b_2E))\tilde{\gamma}_{CO}\end{aligned} \tag{B.8}$$

then obtaining

$$\tilde{\gamma}_{CO} = \left[\frac{\left({R_{ct,1}}^{-1} - {R_{ct,2}}^{-1}\right)}{\Gamma Fj\omega + K_1\exp(b_1E) + K_2\exp(b_2E)}\right]\tilde{E}. \tag{B.9}$$

Being the Faradaic current density a function of surface coverage and potential, the oscillating current density is given by

$$\tilde{j}_F = \left.\frac{\partial f}{\partial\tilde{\gamma}_{CO}}\right|_E\tilde{\gamma}_{CO} + \left.\frac{\partial f}{\partial E}\right|_{\tilde{\gamma}_{CO}}\tilde{E}$$

thus, it can be written as

$$\tilde{j}_F = \tilde{j}_1 + \tilde{j}_2 = \left(R_{ct,1}{}^{-1} + R_{ct,2}{}^{-1}\right)\tilde{E} + \left(K_2\exp(b_2E) - K_1\exp(b_1E)\right)\tilde{\gamma}_{CO}. \tag{B.10}$$

The admittance is expressed as in Equation (11), thus it can be rewritten as follows:

$$Y = \frac{1}{R_{ct}} + \frac{\left(K_2\exp(b_2E) - K_1\exp(b_1E)\right)\left(R_{ct,1}{}^{-1} - R_{ct,2}{}^{-1}\right)}{\Gamma F j\omega + K_1\exp(b_1E) + K_2\exp(b_2E)} \tag{B.11}$$

where $R_{\mathrm{ct}}{}^{-1} = R_{\mathrm{ct},1}{}^{-1} + R_{\mathrm{ct},2}{}^{-1}$.

As consequence, the admittance can be expressed in the form reported in Equation (12) that we recall here:

$$Y = \frac{1}{R_{ct}} + \frac{A}{j\omega + B}.$$

where A can have both positive or negative sign depending on k_1, k_2, and E values. If $A > 0$, the electrical circuit providing the impedance response equivalent to Equation (12) is a charge transfer resistance R_{ct} in parallel with an inductance in series with a resistance (see inset of Figure 5). The inductance assumes the value of $1/A$ and the resistance of A/B. On the contrary, if $A > 0$, the impedance can be written as follows:

$$Z = R_{ct} + \frac{\frac{-AR_{ct}}{B + AR_{ct}}}{\frac{j\omega}{B + AR_{ct}} + 1}. \tag{B.12}$$

The electrical circuit providing the impedance response equivalent to the same Equation (12) is a charge transfer resistance in series with a parallel between a capacitance and a resistance. The capacitance assumes the value of $-1/AR_{\mathrm{ct}}$ and the resistance the value of $-AR_{\mathrm{ct}}{}^2/(B + AR_{\mathrm{ct}})$.